NJC

Accepted Manuscript

This is an *Accepted Manuscript*, which has been through the Royal Society of Chemistry peer review process and has been accepted for publication.

Accepted Manuscripts are published online shortly after acceptance, before technical editing, formatting and proof reading. Using this free service, authors can make their results available to the community, in citable form, before we publish the edited article. We will replace this *Accepted Manuscript* with the edited and formatted *Advance Article* as soon as it is available.

You can find more information about *Accepted Manuscripts* in the Information for Authors.

Please note that technical editing may introduce minor changes to the text and/or graphics, which may alter content. The journal's standard Terms & Conditions and the Ethical guidelines still apply. In no event shall the Royal Society of Chemistry be held responsible for any errors or omissions in this *Accepted Manuscript* or any consequences arising from the use of any information it contains.

ROYAL SOCIETY OF CHEMISTRY

www.rsc.org/njc

NJC

ARTICLE

Interconnected core–shell pyrolyzed polyacrylonitrile@sulfur/carbon nanocomposites for rechargeable lithium–sulfur batteries

Received 00th January 20xx,
Accepted 00th January 20xx

DOI: 10.1039/x0xx00000x

www.rsc.org/

Zhi Chang,[†] Hui Dou,[†]* Bing Ding, Jie Wang, Ya Wang, Guiyin Xu and Cheng Li

Elemental sulfur has attracted great interest for rechargeable batteries because of its high theoretical specific capacity and low cost. However, sulfur electrodes still suffer from rapid capacity fading, which is mainly caused by the undesirable dissolution of polysulfide intermediates and the irreversible deposition of discharge products. In this work, we describe an interconnected core–shell pyrolyzed polyacrylonitrile@carbon/sulfur (pPAN@C/S) nanostructure for high-performance lithium–sulfur batteries. The sulfur was firstly confined in a conductive porous carbon host as C/S to enhance the conductivity of sulfur, constrain polysulfide intermediates and alleviate volume expansion during cycling. Then a conductive pPAN shell was formed by annealing of PAN absorbed on the surface of C/S at 300 °C to further prevent polysulfide intermediates from dissolution by additional physical and chemical barrier. Meanwhile, the conductive pPAN shell could prevent the irreversible deposition of insoluble discharge products and then leading to improved cyclic stability. The interconnected core–shell pPAN@C/S electrodes exhibits a very high initial discharge capacity of 1269 mAh g^{-1} at 0.5 C and shows excellent cycling stability and rate performance.

1. Introduction

Due to the increasing demand of high energy for portable electronic and electrical applications, it is of great significance to develop high-energy-density rechargeable batteries.[1,2] Elemental sulfur has the highest specific capacity among all the known cathode materials for rechargeable lithium batteries except for Li–O_2 cathode.[3,4] Assuming the sulfur could be completely transformed to Li_2S, the Li–S battery can achieve a theoretical specific capacity of 1675 mAh g^{-1} and 2600 W h kg^{-1}, respectively. Elemental sulfur also shows advantages of low cost, natural abundance and environmental friendliness.[5] There are still a number of challenges, however, for sulfur electrode hindering the commercialization of Li–S battery:[6,7] 1) the low electrical conductivity of element sulfur (5×10 g^{-30} S cm^{-1} at 25 °C); 2) the dissolution of polysulfide intermediates in the organic electrolytes; 3) the large volume expansion of sulfur electrode during cycling. All these issues lead to a low utilization of active material, low Coulombic efficiency, and poor cycle life of the sulfur electrode.[8-10]

To solve these problems, confining elemental sulfur into a conductive matrix is an effective strategy. To date, various matrices, such as porous carbon materials,[11-26] conductive polymer materials[27-29] and metal oxides,[30-34] were applied to improve the electrical conductivity of sulfur cathodes and to some extent reduce the dissolution of lithium polysulfides.[23,24] For example, Nazar *et al*.[35], reported that ordered mesoporous carbon CMK-3 could trap sulfur species during charge/discharge process. The electrode with sulfur confined in the meso-channels of CMK-3 exhibited a capacity of about 1000 mAh g^{-1} after cycling for 20 cycles. Our group reported that by confining polymeric sulfur in the porous carbon, an initial specific capacity of 1105 mAh g^{-1} was obtained and a capacity of 889 mAh g^{-1} was still sustained even after 100 cycles.[26] The encapsulation technology, however, can only reduce but not totally eliminate the dissolution of polysulfides. Part of the polysulfides still could escape from the matrix. To further prolong the cycling performance of sulfur electrode, core–shell and/or yolk–shell nanostructures were designed. Yang *et al*.[36], for example, prepared polydopamine-coated carbon–sulfur nanocomposite which could confine the sulfur particles inside the hollow carbon spheres, thus immobilizing the polysulfides and improving the cycling stability. However, host materials and the coating layer normally make no contribution to the capacity. Therefore, these methods undoubtedly sacrifices energy density of the Li–S batteries. An alternative route to enhance the stability is using sulfurized carbons. Wang *et al*.[27] reported that pyrolyzed polyacrylonitrile/sulfur (PAN–S) composites exhibited enhanced cycling stability and rate performance, especially after introducing additional electrically conductive material into the composite, such as carbon nanotubes (CNTs).[37,38] For example, core-shell nanostructured PAN-S@CNTs composite retained a reversible discharge capacity of 697 mAh g^{-1} after 50 cycles at 0.1 C. But massive inactive composites coated on elemental sulfur inevitably lower the sulfur content of electrodes.

In this work, the interconnected core-shell nanocomposites

Jiangsu Key Laboratory of Materials and Technology for Energy Conversion, College of Material Science and Engineering, Nanjing University of Aeronautics and Astronautics, Nanjing, 210016, P. R. China.

Electronic Supplementary Information (ESI) available: [SEM images, TGA curves, XRD patterns, XPS spectra, electrochemical performance]. See DOI:10.1039/x0xx00000x

[†] Both authors contributed equally to this work.

of pyrolyzed polyacrylonitrile@carbon/sulfur (pPAN@C/S) have been prepared by coating and annealing of polyacrylonitrile(PAN) on the C/S composites The porous carbon core employed there acts as a high conductive host material which could also physically confine sulfur species and alleviate volume expansion during cycling. Then the pPAN shell was formed by annealing of PAN absorbed on the surface of C/S at 300°C to further prevent polysulfides from dissolution by additional physical and chemical barrier[38]. Meanwhile, the conductive polymer could prevent the irreversible deposition of insoluble discharge products and then leading to improved cyclic stability.[25,26] We show that, as electrode materials for Li–S batteries, the interconnect core–shell pPAN@C/S exhibited high initial discharge capacity, excellent cycling stability and rate performance.

2. Experimental

2.1 Preparation of C/S and pPAN@C/S composites

The C/S composites with a sulfur content of 70 wt% was prepared through a simple melt-diffusion method as described in previous reports.[35] Typically, 150 mg commercial conductive porous carbon (Ketjenblack EC600JD, KJC) and 350 mg sublimed sulfur (chemical grade) were ground together, and heated at 155 °C for 12 h. Then the PAN@C/S composites were prepared by adsorbing of PAN onto the outer surface of the C/S. In detail, 50 mg C/S composites and PAN (5, 10 and 20 mg.) were dispersed in 5 ml N,N-dimethylformamide (DMF), and sonicated for 15 minutes, respectively. Then the PAN solution was added into above C/S suspension, and sonicated for another 15 minutes. After the mixture was stirred over night at room temperature, the DMF was evaporated at 80 °C. The PAN@C/S composites prepared with different mass ratios of PAN to C/S (1:10, 2:10 and 4:10) were noted as PAN^{1}@C/S, PAN^{2}@C/S and PAN^{4}@C/S. Finally, the obtained PAN@C/S composites were annealed at 300 °C in argon (Ar) environment for 2 h to yield corresponding pPAN^{1}@C/S, pPAN^{2}@C/S and pPAN^{4}@C/S.

2.2 Material Characterization

The morphology of the as-prepared C/S and pPAN@C/S composites were characterized by X-ray diffraction measurement (XRD, Bruker-AXS D8 DISCOVER using Cu Kα radiation), scanning electron microscopy (SEM,JEOL JSM-6380LV FE-SEM) and transmission electron microscopy (TEM, FEI, Tecnai-20),respectively. The X-ray photoelectron spectroscopy (XPS) analysis was performed on a Perkin-Elmer PHI 550 spectrometer with Al Kα (1486.6 eV) as the X-ray source. Fourier transform infrared (FT-IR) spectra were recorded with a model 360 Nicolet AVATAR FT-IR spectrophotometer by using pressed KBr pellets. Thermogravimetric analysis (TGA) was conducted on a TG-DSC instrument (NETZSCH STA 409 PC) under nitrogen protection at a heating rate of 10 °C min^{-1} from 30 to 500 °C.

2.3 Electrochemical measurements

The working electrodes were prepared by mixing 70 wt. % of active materials, 20 wt. % of carbon black, and 10 wt. % of polyvinylidene fluoride (PVDF) in N-methyl-2-pyrrolidone (NMP) solvent. The slurry was spread uniformly on an aluminum foil current collector. The work electrodes were dried in a vacuum oven at 60 °C overnight. The areal mass loading of sulfur is about 0.6-0.8 mg/cm^{2}. CR2016 coin cells were assembled in an argon-filled glove box, in which both the moisture and oxygen contents were controlled to be less than 1 ppm. Lithium foil was used as the counter electrode. The electrolyte was 1M lithium bis(trifluoromethanesulfonyl)-imide (LiTFSI) and 0.1 M $LiNO_3$ in a mixed solvent of 1,3-dioxolane (DOL) and 1,2-dimethoxyethane (DME) with a volume ratio of 1:1. The volume of the electrolyte added in each cell is 45 µL. The coin cells were galvanostatically charged/discharged at different current densities between 1.7 and 3.0 V (vs. Li/Li^{+}) by using a CT2001A cell test instrument (LAND Electronic Co.) Cyclic voltammetry (CV) and electrochemical impedance spectra (EIS) were conducted with a CHI 600A electrochemical workstation at a scanning rate of 0.2 mV s^{-1}.

3. Results and discussion

3.1 Preparation and characterization of the pPAN@C/S

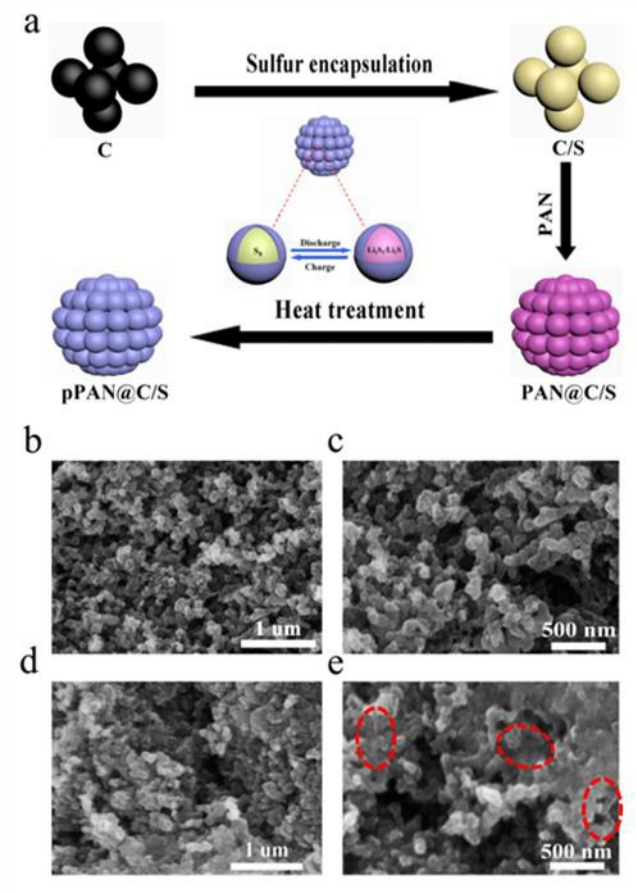

Fig. 1 (a) Schematic illustration of the preparation route of the pPAN@C/S composites and SEM images of (b, c) C/S and (d, e) pPAN^{1}@C/S composites.

The preparation route of the pPAN@C/S core–shell nanostructure is schematically presented in Fig. 1a. Firstly, elemental sulfur was encapsulated into porous carbon nanoparticles to form C/S composites, which could provide the physical confinement/immobilization of sulfur and efficaciously trap the soluble polysulfides species in the pores and improve the electronic conductivity of the cathode. Then PAN was adsorbed onto the surface of the C/S dispersed in DMF by set for overnight to produce core–shell PAN@C/S composites. After thermal treatment at 300 °C, the PAN was cyclized through the interaction of –CN functional groups and then dehydrogenated by sulfur, finally forming a thermally stable hetero cyclic composites as shown in Fig. S1. The conductive pyrolyzed PAN covalently bound with sulfur species S_x (x =2–3), which serves to further restrict the dissolution of polysulfides by physical and chemical interaction and improve stability of sulfur cathode during electrochemical cycling.[39] The morphology of pPAN[1]@C/S composites was characterized by scanning electron microscopy (SEM) and transmission electron microscopy (TEM). As shown in the Fig. 1b and c, the C/S composites show a spherical morphology. The size of particles is approximately 100 nm. Large sulfur particles or agglomerates are not observed, indicating that elemental sulfur was totally encapsulated in the nanopores of the carbon host. And the PAN[1]@C/S composites show a similar morphology with C/S composites (Fig S2). By contrast, the pPAN[1]@C/S composites show obviously different morphology (Fig. 1d, e). The nanoparticles agglomerate with each other and then form some interconnected particles. And the surface of pPAN[1]@C/S composites is smoother and particle size is bigger than that of the C/S composites (highlighted by red circles in Fig. 1e), indicating successful coating of pPAN on the surface of C/S.

In the TEM images of the pPAN[1]@C/S (Fig. 2a and b), the core–shell nanostructure can be found clearly. The light-color area is the dehydrogenated pPAN whereas the dark-color area is the C/S. No excessive sulfur is found, which further confirms that sulfur was successfully infused in the inner space of the carbon host instead of the exterior. The elemental mapping images reveal similar distribution of elemental C, S and N, suggesting a uniform distribution of sulfur and pPAN in the composites (Fig. 2c).

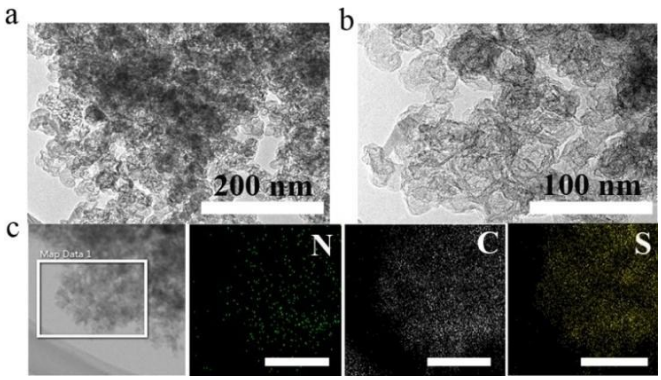

Fig. 2 TEM and EDS images of the pPAN[1]@C/S; (a, b) TEM images and the corresponding elemental mapping for (c) C, N and S.

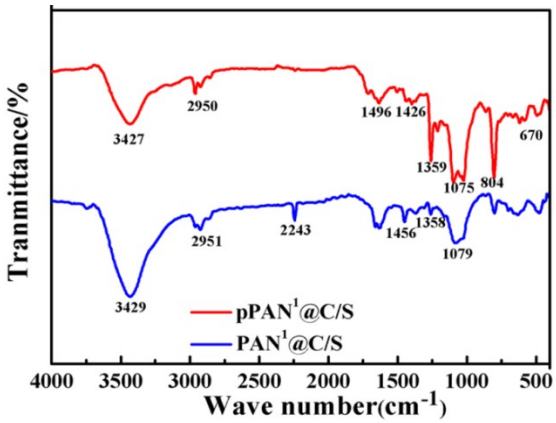

Fig. 3 FT-IR spectra of the PAN[1]@C/S.

The materials were further studied with Fourier transform infrared (FT-IR) spectra and X-ray photoelectron spectroscopy (XPS). In the FT-IR spectrum of the PAN[1]@C/S, two characteristic peaks at 2243cm^{-1} and 1456 cm^{-1} represent the -CN and -CH_2 groups respectively.[27] After being annealed at 300 °C, the two peaks disappear in the FT-IR of pPAN[1]@C/S, and new absorption bands at 1426 cm^{-1}and 804 cm^{-1}appear, which indicates the formation of a heterocyclic compound during heat treatment (Fig. 3).[28] Table S1 shows the detailed FT-IR information of pPAN[1]@C/S. The XPS spectra in the C 1s region (Fig S3) for pPAN[1]@C/S reveal that the C 1s band can be deconvoluted into two peaks at 284.6 eV and 286.4 eV, assigned to sp^2 type C–C and C–S or C–N.[39] The S 2p spectra for the pPAN[1]@C/S show an overlapped band with two shoulder bands (Fig 4a). The main S $2p^{3/2}$ peak at 163.8 eV, slightly lower than the binding energy of elemental sulfur (164.0 eV), is consistent with the presence of C–S bonds in the composite. Another S $2p^{3/2}$ peak at 165.4eV can be attributed to S–S bonds.[40] The XPS spectra in the N1s region display two peaks centered at 398.2 and 401.0 eV, corresponding to the pyridinic and quaternary N, respectively (Fig 4b).[41] These nitrogen bonds are ascribed to the formation of a heterocyclic compound which in turn supports the conclusion of the FT-IR spectrum of the pPAN[1]@C/S. The sulfur contents in the C/S, pPAN[1]@C/S, pPAN[2]@C/S and pPAN[4]@C/S were measured by thermogravimetric analysis (TGA) (Fig. S4 and S5). The TGA curve of C/S shows a 70 wt% weight loss between 160 and 380 °C and the TGA curves of three different pPAN@C/S composites show about 56, 52 and 46% weight loss between 160 and 320 °C, which corresponds to the release of sulfur in the composites, respectively. The X-ray diffraction (XRD) patterns of sulfur, PAN, C/S andpPAN[1]@C/S are shown in Fig. S6. The peaks of crystalline sulfur in the XRD pattern of the C/S totally disappear (Fig. S6a), suggesting that sulfur was uniformly immersed into the nanopores of carbon host. After being annealed, the typical peaks of PAN are not observed in the XRD pattern of the pPAN[1]@C/S (Fig. S6b), which indicates that PAN has been partially dehydrogenated by sulfur, and then form a conductive heterocyclic structure.

3.2 Electrochemical performance of the pPAN@C/S.

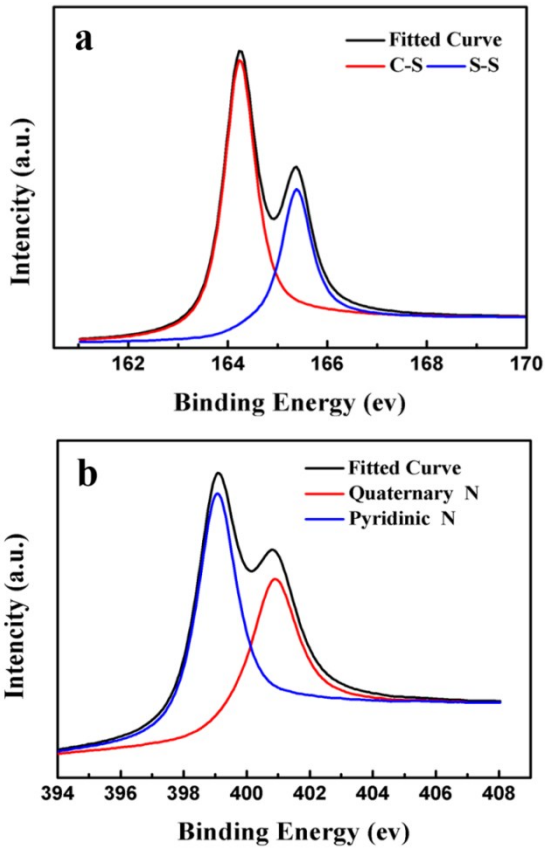

Fig. 4 (a) S 2p, (b) N 1s XPS of the pPAN[1]@C/S.

The electrochemical performance of the pPAN@C/S and C/S were compared to investigate the effect of the pPAN coating layer on the electrochemical performance of the pPAN@C/S as electrode materials. Fig. 5a compares the cycle performance and columbic efficiency of different pPAN@C/S and C/S at a current rate of 0.5 C (1 C=1675 mAh g^{-1}). Clearly, the pPAN[1]@C/S electrode shows the best cycling performance. After 100 cycles, the pPAN[1]@C/S electrode can still remain a capacity of 817 mAh g^{-1} based on the mass of sulfur in the composites, much better than its C/S counter-part. For the pPAN[2]@C/S electrode, the initial discharge capacity is about 901 mAh g^{-1}. After 100 cycles, the capacity is only 702 mAh g^{-1}. As for the pPAN[4]@C/S electrode, the initial discharge capacity is about 840 mAh g^{-1}. After 100 cycles, the capacity is only about 442 mAh g^{-1}. Meanwhile, all these three cathodes exhibit nearly 100% Columbic efficiency during charge-discharge process. The best electrochemical stability of pPAN[1]@C/S could be due to the proper electric conductivity since too much pPAN containing in the composites might bring negative effect to electrodes. Thus, the pPAN[1]@C/S was adopted to investigate the effect of the pPAN coating layer on the electrochemical performance as electrode materials. Fig. 5b shows the galvanostatic charge/discharge profiles of pPAN[1]@C/S electrode for the first three cycles at 0.5 C. During the discharge process, the high plateau at around 2.2 V is assigned to the reduction from S_8 to soluble long-chain polysulfides while the low plateau at about 2.0 V is assigned to the transformation from long-chain polysulfides to short-chain Li_2S_2/Li_2S. The plateau at around 2.2 V can be attributed to the oxidation of Li_2S and Li_2S_2 to Li_2S_8[11,12]. It is consistent with the cyclic voltammetry analysis in Fig. 5c. The initial specific capacity of pPAN[1]@C/S is about 1269 mAh g^{-1} while the following two specific capacities are 1123 mAh g^{-1} and 1076 mAh g^{-1}. Fig S7 shows the galvanostatic charge-discharge profiles of the C/S at 0.5 C. The specific capacities of the C/S electrode at 0.5 C for the first three cycles are 746.7, 743.1 and 731.5 mAh g^{-1}, much lower than those of pPAN[1]@C/S. Cyclic voltammograms of the pPAN[1]@C/S (Fig 5c) and C/S (Fig S8) cathodes were investigated at a scan rate of 0.2 mV s^{-1} and potential window of 1.7 and 3.0 V. It was found from the CVs that there are two cathodic peak potentials at 2.04 and 2.31 V for the C/S composites. According to the multiple reaction mechanism of sulfur, the two well-defined reduction peaks could be assigned to the multi-step reduction of elemental sulfur. The first cathodic peak at about 2.31 V (vs. Li/Li^+) is contributed to the transformation of linear sulfur units to long chain polysulfides Li_2S_x ($4 \leqslant x \leqslant 8$). The sequential cathodic peak at 2.04 V corresponds to further reduction of long-chain polysulfides to Li_2S_2/Li_2S. The anodic peak at about 2.39 V corresponds to the oxidation of Li_2S_2/Li_2S to Li_2S_8. By contrast, the sharp redox peaks of pPAN[1]@C/S were moved up to 2.08 and 2.32 V (vs. Li/Li^+), indicating the fast kinetics and less reaction species during cycling, and confirming a relatively low potential polarization and good reversibility after coating pPAN on the C/S composites.[42] Fig. 5d compares the cycle performance of C/S and pPAN[1]@C/S at 1 C. The pPAN[1]@C/S electrode shows better cycling performance while its C/S counter-part has much poor cycling performance.

Fig 5e compares the capacity contribution from the low and high plateaus of both pPAN[1]@C/S and C/S electrodes. It has been reported that the upper plateau reactions are the main causes of the performance deterioration in the Li–S cell system.[43] As shown in the graph, although the upper plateaus of both pPAN[1]@C/S and C/S electrodes keep shrinking with increasing cycle number, the shrinkage of the pPAN[1]@C/S electrode is much less than that of the C/S electrode, which implies that the utilization of active material is greatly improved. The rate performance of the pPAN[1]@C/S and C/S has been depicted in Fig. 5f. At rates of 0.2, 0.5, 1, 2 and 0.2C, the capacities of the pPAN[1]@C/S composites are 950, 808, 725, 561 and 801mAh g^{-1}. When the current density was switched abruptly from 2 to 0.2 C again, the original capacity was largely recovered, indicating robustness and stability of the cathode material. However, by sharp contrast, the maximum capacities of the C/S composites are only 511.3, 371.2, 306.6, 252.1 and 352.8 mAh g^{-1} at rates of 0.2, 0.5, 1, 2 and 0.2 C, demonstrating a much poorer rate performance. Notably, the cycling performance of the pPAN[1]@C/S is much better than that of PAN–S composites reported by Wang *et al*. The pPAN[1]@C/S deliver a specific capacity of 650 mAh g^{-1} at 1 C after 50 cycles, while the PAN–S composites only maintain a capacity of about 560 mAh g^{-1} at 0.5 C after 50 cycles.[25]

The enhanced electrochemical performance of the pPAN[1]@C/S could be ascribed to the synergistic restriction of S by both porous carbon host and conductive pPAN layer. The nanopores in the porous carbon not only act as polysulfides

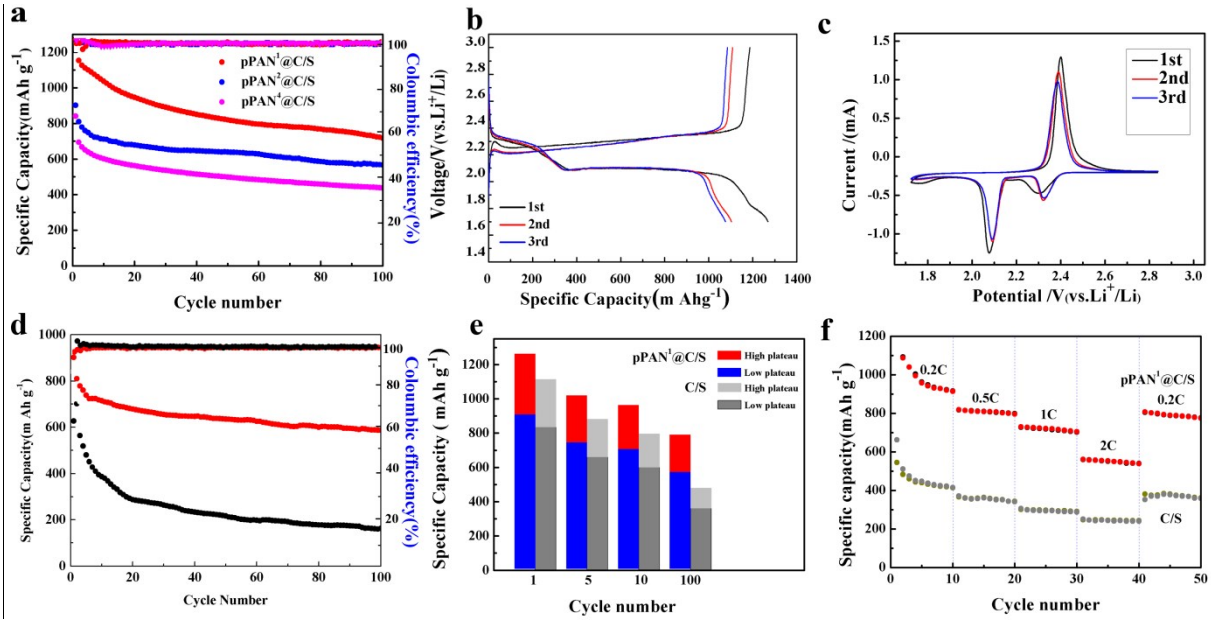

Fig. 5 (a) Cycling performances of pPAN@C/S electrode with different PAN content and the pure C/S electrode at 0.5 C. (b) Galvanostatic charge-discharge profiles of pPAN[1]@C/S for the first three cycles at 0.5 C. (c) CV curves at a scanning rate of 0.2 mV/S of pPAN[1]@C/S electrode. (d) Cycling performance of pPAN[1]@C/Sand C/S at 1 C. (e) Capacity contribution from the low and high plateau of both pPAN[1]@C/S and C/S at 0.5 C. (f) Rate capability of the pPAN[1]@C/S and C/S cathodes cycled at current densities from 0.2 C to 2 C.

reservoir, to physically confine sulfur and the soluble products, but also alleviate the volume expansion during cycling. In addition, the pPAN layer could also prevent polysulfide intermediates from dissolution as a physical barrier. Moreover, the pPAN layer could further provide additional chemical confinement to block the diffusion of polysulfides and prevent the irreversible deposition of soluble discharge products.

The reconstituted N functional groups in the shell are efficient in trap intermediate higher-order lithium polysulfides through the strong S_xLi–N interactions via the N lone-pair electrons.[39] Therefore, the re-deposition of Li_2S/Li_2S_2 upon discharge-charge process has been largely improved, thus leading to excellent cyclic stability and high-rate performance. In addition, in this work, we emphasize that we could prepare high-performance electrode materials for Li–S batteries by using commercial porous carbon and PAN. The as-prepared pPAN[1]@C/S composites exhibit comparable electrochemical performance with other nanostructured electrode materials, which usually were prepared through complex and time-consuming template-method or chemical activation.[26,44–46]

In order to better understand the role of pPAN shell to the irreversible deposition of Li_2S/Li_2S_2 on the surface of electrodes, morphologies of the C/S and pPAN[1]@C/S electrodes after 100 cycles (at fully charged state) were investigated by SEM. As shown in Fig. 6a, piles of irregular discharge products are irreversibly deposited on the surface of C/S electrode. The chemically inactive discharge products can not only attribute to the loss of active material, but also make some undesirable effects in decreasing the reactive sites. Both of two effects could result in the fading in capacity. By contrast, the pPAN[1]@C/S electrode has a totally different morphology and stay nearly unchanged after cycling, implying that the irreversible deposition of discharge products on the surface of electrode is effectively suppressed (Fig. 6b).

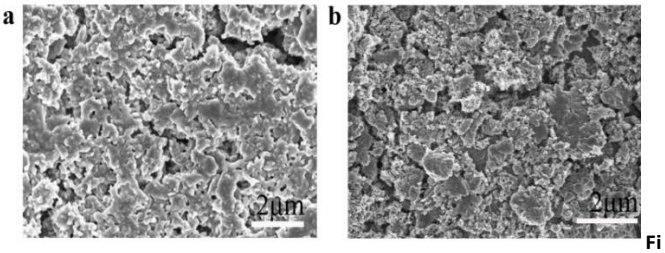

Fig. 6 SEM images of (a) C/S and (b) pPAN[1]@C/S electrodes after cycling for 100 cycles.

Fig. 7 compares the EIS spectra of the C/S and pPAN[1]@C/S electrodes after 100 cycles. The EIS is composed of a semicircle in the high-frequency domain and a straight line in the low-frequency region. The semicircle in the high-frequency domain corresponds to the charge-transfer process, and the straight line in the low-frequency domain corresponds to a semi-infinite Warburg diffusion process. Obviously, the pPAN[1]@C/S electrode shows lower charge-transfer resistance and Warburg diffusion resistance and charge-transfer resistance, indicating the more rapid electronic/ionic transport in the pPAN[1]@C/S electrode. All of this can be attributed to the more uniform dispersion of the active material and the conductive N function contained pPAN polymer in the pPAN[1]@C/S electrode which can trap insoluble discharge

products and then suppress the irreversible deposition of insoluble products. Therefore, the aggregation of insulated

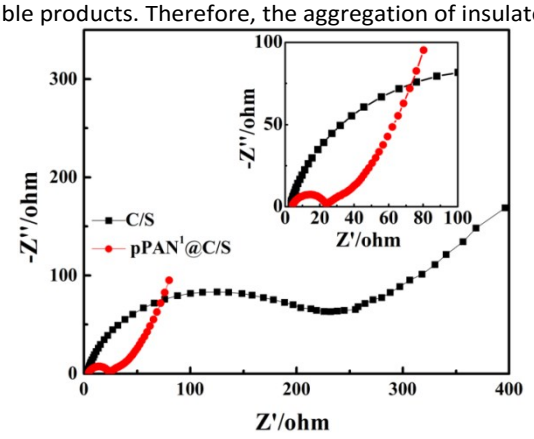

Fig. 7 EIS spectra of C/S and pPAN[1]@C/S electrodes after 100 cycles. The inset shows the spectra at high-frequency region.

Li_2S_2 and Li_2S on the surface of electrode during cycling could be significantly suppressed due to the pPAN coated C/S composites.

Conclusion

In summary, the interconnected core–shell pPAN@C/S composites have been synthesized as cathode materials for high-performance Li–S batteries. For the pPAN@C/S composites, the conductive porous carbon could improve the electrical conductivity. Meanwhile, the porous carbon and pPAN polymer shell could not only act as small nanoreactors to restrict the dissolution of lithium polysulfides in organic electrolyte, but also alleviate the volume expansion during cycling process. Moreover, the pPAN polymer shell further guarantees a more reversible charge-discharge process of active material by the chemical binding to the polysulfides. Benefited from both the entrapment of the polysulfides by the carbon core and pPAN polymer shell, the pPAN@C/S electrode shows high specific capacity with excellent cycling stability and rate performance. This interconnected core–shell pPAN[1]@C/S electrode exhibited a very high initial capacity of 1269 mAh g^{-1} at 0.5 C. This work demonstrated that the pPAN@C/S electrode has a great potential to be used in low-cost and high-energy Li–S batteries and provides a common method to prepare polymeric C/S composites.

Acknowledgements

This work was supported by the National Basic Research Program of China (973 Program) (No. 2014CB239701), National Natural Science Foundation of China (No. 21173120, 51372116), Natural Science Foundation of Jiangsu Province (BK2011030, BK20151468) and the Fundamental Research Funds for the Central Universities of NUAA (NP2014403). Z. Chang is grateful to the Foundation of Graduate Innovation Center in NUAA (kfjj20150612).

Notes and references

1. J. M. Tarascon, M. Armand, *Nature*, 2001, 414, 359.
2. P. G.Bruce, S. A. Freunberger, L. J.Hardwick and J. M. Tarascon, *Nat. Mater*., 2012, 11, 19.
3. A. Manthiram, Y. Z. Fu and Y. S. Su, *Acc. Chem. Res*., 2013, 46, 1125.
4. P. G. Bruce, L. J. Hardwick and K. M. Abraham, *MRS Bull*., 2011, 36, 506.
5. D.-W. Wang, Q. Zeng, G. Zhou, L. Yin, F. Li, H.-M. Cheng, I. R. Gentle and G. Q. M. Lu, *J. Mater. Chem. A*, 2013, 1, 9382.
6. V. Etacheri, R. Marom, R. Elazari, G. Salitra and D. Aurbach, *Energ Environ Sci*., 2011, 4, 3243.
7. Y. Yang, G. Y. Zhang and Y. Cui, *Chem. Soc. Rev.* 2013, 42, 3018.
8. T. Bandhauer, S. Garimella and T. Fuller, *J Electrochem Soc*., 2011, 158, R1.
9. S. Evers and L. F. Nazar, *Acc. Chem. Res*., 2013, 46, 1135.
10. G. Y. Xu, B. Ding, L. F. Shen, P. Nie, J. P. Han and X. G. Zhang, *J. Mater. Chem. A*, 2013, 1, 4490.
11. J. J. Chen, X. Jia, Q. J. She, C. Wang, Q. A. Zhang, M. S. Zheng and Q. F. Dong, *Electrochim. Acta*., 2010, 55, 8062.
12. B. Ding, C. Z. Yuan, L. F. Shen, G. Y. Xu, P. Nie, Q. X. Lai and X. G. Zhang, *J. Mater. Chem. A*, 2012, 1, 1096.
13. J. J. Chen, Q. Zhang, Y. N. Shi, L. L. Qin, Y. Cao, M. S. Zheng and Q. F. Dong, *Phys. Chem. Chem. Phys*.,2012,14, 5376.
14. R. Elazari, G. Salitra, A. Garsuch, A. Panchenko and D. Aurbach, *Adv. Mater*., 2011, 23, 5641.
15. J. C. Guo, Y. H. Xu and C. S. Wang, *Nano Lett*., 2011, 11, 4288.
16. G. He, X. L.Ji and L. F. Nazar, *Energ Environ. Sci*., 2011, 4, 2878.
17. F. R. Qing, K. Zhang, J. Fang, *New J. Chem*., 2014, 38, 4549.
18. L. Ji, M. Rao, H. Zheng, L. Zhang, Y. Li, W. Duan, J. Guo, E. J. Cairns and Y. Zhang, *J. Am. Chem. Soc*., 2011, 133, 18522.
19. Z. Li, Y. Jiang, L. Yuan, Z. Yi, C. Wu, Y. Liu, P. Strasser and Y. Huang, *ACS Nano*., 2014, 8, 9295.
20. D.-W. Wang, G. M. Zhou, F. Li, K. H. Wu, G. Q. Lu, H. M. Cheng and I. R. Gentle, *Phys. Chem. Chem. Phys*., 2012, 14, 8703.
21. H. L. Wang, Y. Yang, Y. Y. Liang, J. T. Robinson, Y. G. Li, A. Jackson, Y. Cui and H. J. Dai, *Nano Lett*., 2011, 11, 2644.
22. C. F. Zhao, B. W. Hao, C. Z. Yuan, Z. P. Guo and X. W. Lou *Angew. Chem Int. Ed*, 2012, 124, 9730.
23. G. Y. Zheng, Y. Yang, J. J. Cha, S. S. Hong and Y. Cui, *Nano Lett*., 2011, 11, 4462.
24. P. Zhu, J. Song, D. Lv, D. Wang, C. Jaye, D. A. Fischer, T. Wu and Y. Chen, *J Phys Chem C*., 2014, 118, 7765.
25. Z. Li, J. T. Zhang, Y. M. Chen, J. Li, X. W. Lou, *Nat. Commun*., 2015, 6, 8850.
26. B. Ding, Z. Chang, G. Xu, P. Nie, J. Wang, J. Pan, H. Dou and X. Zhang, *ACS Appl. Mater. Interfaces*, 2015, 7, 11165.
27. J. L. Wang, J. Yang, C. R. Wan, K. Du, J. Y. Xie and N. X. Xu, *Adv. Funct Mater.*, 2003, 13,487.
28. J. L. Wang, J. Yang, J. Y. Xie and N. X. Xu, *Adv. Mater.*, 2002, 14, 963.
29. M. J. Wang, W. K. Wang, A. B. Wang, K. G. Yuan, L. X. Miao, X. L. Zhang, Y. Q. Huang, Z. B. Yu and J. Y. Qiu, *Chem. Commun*., 2013, 49, 10263.
30. *Z. Liang, G. Zheng, W. Li, Z. Wei Seh, H. Yao*, K. Yan, D. Kong and Y. Cui, *ACS Nano*, 2014, 8, 5249.

31. Q. Pang, D. Kundu, M. Cuisinier and L. F. Nazar, *Nat.Commun*., 2014, 5, 4759.
32. X. Liang, C. Hart, Q. Pang, A. Garsuch, T. Weiss and L. F. Nazar, *Nat.Commun*., 2015, 6,5682.
33. Z. W. Seh, W. Li, J. J.Cha, G.Zheng, Y. Yang, M. T. McDowell, P-C. Hsu and Y. Cui, *Nat.Commun*., 2013, 4, 1331.
34. Z. Li, J. Zhang and X. W. Lou, *Angew. Chem Int. Ed*, 2015, 54:12886.
35. X. L. Ji, K. T. Lee and L. F. Nazar, *Nat. Mater*., 2009, 8, 500.
36. W. Zhou, X. Xiao, M. Cai and L. Yang, *Nano Lett*., 2014, 14, 5250.
37. L. C. Yin, J. L. Wang, J. Yang and Y. N. Nuli, *J. Mater. Chem.*, 2011, 21, 6807.
38. L. C. Yin, J. L. Wang, F. J. Lin, J. Yang and Y. N. Nuli, Energy Environ. Sci., 2012, 5, 6966.
39. S. Wei, L. Ma, K. E. Hendrickson, Z. Tu and L. A. Archer, *J. Am. Chem. Soc*., 2015, 137, 12143.
40. J. Fanous, M. Wegner, J. Grimminger, Ä. Andresen and M. R. Buchmeiser, *Chem Mater*., 2011, 23, 5024.
41. Y. Qin, J. Yuan, J. Li, D. Chen, Y. Kong, F. Chu, Y. Tao and M. Liu, *Adv. Mater*., 2015, 27, 5171.
42. G. C.Li, G. R. Li, S. H. Ye and X. P. Gao, *Adv. Energy Mater*., 2012,2, 1238−1245
43. Y. S. Su, Y. Fu, T. Cochell and A. Manthiram, *Nat.Commun*., 2013, 4, 2985.
44. G. Xu, J. Yuan, X. Tao, B. Ding, H. Dou, X. Yan, Y. Xiao and X. Zhang, Nano Res., 2015, 8, 3066–3074.
45. G. Xu, B. Ding, L. Shen, P. Nie, J. Han and X. Zhang, *J. Mater. Chem. A*, 2013, 1, 4490–4496.
46. G. Xu, B. Ding, P. Nie, L. Shen, H. Dou and X. Zhang, *ACS applied materials & interfaces*, 2013, 6, 194-199.

Interconnected core–shell pyrolyzed polyacrylonitrile@sulfur/carbon nanocomposites have been prepared and adapted as the cathode materials to prevent the irreversible deposition of insoluble discharge products and then leading to improved cyclic stability for lithium–sulfur battery.